ISSN 2959-6157

Numerical simulations on aerodynamic drag reduction of a 25° Ahmed body by jet flow

Dingkai Weng[1, a]

[1]School of Mathematics, Southeast University, Nanjing 210000, China;

Abstract:

In this work, for the aerodynamic characteristics of a 25° Ahmed body, I reduce its aerodynamic drag by adding airflow nozzles at the rear of its model and carrying out computational fluid dynamics simulations and analyses under the flow velocity of the jet port of 10, 20, and 30 m/s respectively, and meanwhile set up the airflow outlets at different locations of the model slope for simulation analyses under the flow velocity of the jet port of 20 m/s. The best up to 16.4% drag reduction rate is achieved in the simulations. The results show that the best drag reduction effect is achieved when the velocity of the jet outlet is 10 m/s. In contrast, the increase in the velocity of the jet outlet will lead to the early separation of the boundary layer, which in turn enhances its aerodynamic drag. As for different airflow outlets, while injecting airflow into the low-pressure region on the slope surface due to the boundary layer separation, moderately moving the jet port downward to enhance the pressure on the front and back of the model can achieve a better drag reduction effect.

Keywords: Ahmed body;Active flow control;Jet flow;Aerodynamic drag reduction.

1. Introduction

In recent years, due to environmental protection and vehicle development needs, the aerodynamic drag of vehicles, as a performance indicator closely related to the fuel consumption of vehicles and their mechanical performance, has been an increasing concern [1]. Relevant studies have pointed out that when the vehicle is travelling, most of the power will be used to overcome the aerodynamic drag of the vehicle. Among the aerodynamic drag forces, the pressure difference drag force generated by the low-pressure region at the rear of the vehicle occupies about 85% [2]. Therefore, reducing differential pressure drag during vehicle driving becomes a key and valuable research topic [3-4]. As for how to simplify the aerodynamic characteristics of vehicle driving and quantify various parameters related to aerodynamics in vehicle driving, Ahmed et al. [5] proposed a simplified model that can be quantitatively described for simulating the aerodynamic situation of vehicles, namely the Ahmed body. With this model, it was pointed out that the main reason for the formation of differential pressure drag in vehicles is the occurrence of boundary layer separation at the rear of the vehicle, which produces a wake return zone [6].

For aerodynamic drag reduction of the Ahmed body, there are two main types of aerodynamic damping: passive damping and active damping The main difference between the two is whether the energy is injected into the vehicle's surroundings or not. The difference between the two is mainly in whether energy is injected into the flow field around the vehicle [7]. Jet flow damping is the most common method of active damping. It is the most common type of active drag reduction. It reduces the aerodynamic drag of a vehicle by injecting air directly into the flow field around the vehicle body to change the aerodynamic characteristics of the vehicle, thus reducing the aerodynamic drag of the vehicle.

For the drag reduction of the Ahmed body, Xue et al. [7] achieved a maximum drag reduction rate of 12.25% by installing a flexible flap at the rear of the body model to improve the tail flow structure and enhance the back pressure. As for the study by Zhou et al. [8], effective drag reduction can also be produced by rounding the tail of the model, but considering the practical application, the rounding of the model is difficult to implement in the online generation of vehicles, so its practical application value is lacking. In terms of active drag reduction, Wang et al. [9] studied the active drag reduction of Ahmed class vehicle body models by plasma flow control, and the overall drag reduction rate of 9.02% can be achieved. However, the plasma generation device is difficult to apply to current vehicles, and there is a potential problem of additional drag caused by the increase in vehicle weight after the addition of the device.

To address the shortcomings of the above study, this project aims to reduce the drag of the Ahmed body with a

back slope angle of 25° by direct injection into the wake area at the top of the sloped back (where most vehicles are often aerodynamically designed to reduce the drag of the vehicle body). Compared to the passive drag reduction design mentioned above, it is more compatible with most vehicle designs because it does not need to change the appearance of the vehicle body itself; at the same time, a normal jetting device is easier to implement on current vehicles than a plasma generator in the current industry.

2. Numerical settings

2.1 Vehicle Model

This paper uses the Ahmed body with a back slope angle of 25°, as shown in Fig. 1, which can be considered to retain the aerodynamic characteristics of the vehicle relatively well even after simplification and quantification of the model. The main body of is a rectangle with a length of 1044 mm, a width of 389 mm and a height of 288 mm. The front is rounded on all sides, and the back of the model has a 222 mm long slope with an angle of 25° to the ground to simulate the rear windscreen of the vehicle. The research topic of this paper is three flat surfaces of 10 mm in length that are separated at the front of the back of the model (P1, P2, and P3 in Fig. 1), and are used as the jet opening.

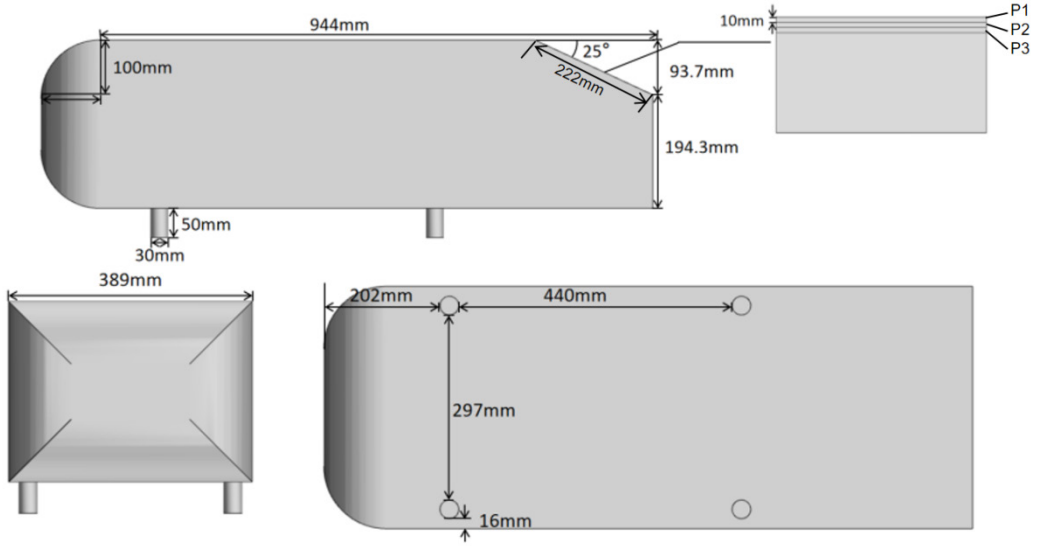

Fig. 1. Ahmed body with a back slope angle of 25°.

2.2 Computational domain and boundary conditions

Fig. 2 illustrates the size of the computational domain for the simulations used in this paper. The length R, width W and height H of the vehicle model are taken as the basic dimensions, and a computational domain is established in which the front and rear are extended by one and six times the length of the vehicle, respectively, and the front side is extended outward by two times the vehicle model and four times the height of the vehicle; the blockage ratio is about 5%. For the computational domain surface, the front and rear planes of the model are set as velocity inlet and pressure outlet, respectively, while the two sides and the upper wall are set as slip wall, and the computational domain floor is set as a no-slip wall in order to conform to the normal conditions of the vehicle travelling on the ground.

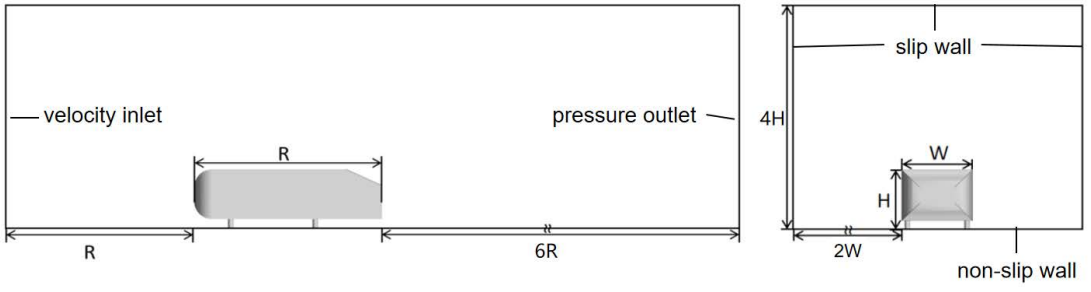

Fig. 2. Computational domain and boundary conditions: (a) front view and (b) side view.

2.3 Computational mesh

Fig. 3 shows the computational mesh in this work. The trimmed meshes are used with the base size of 0.04 m and the encrypted area near the model size of 0.02 m and 0.01 m in that order. As for the boundary layer part, 10 layers with an extension ratio of 1.2 are used to draw. The number of meshes drawn is 2,527,485.

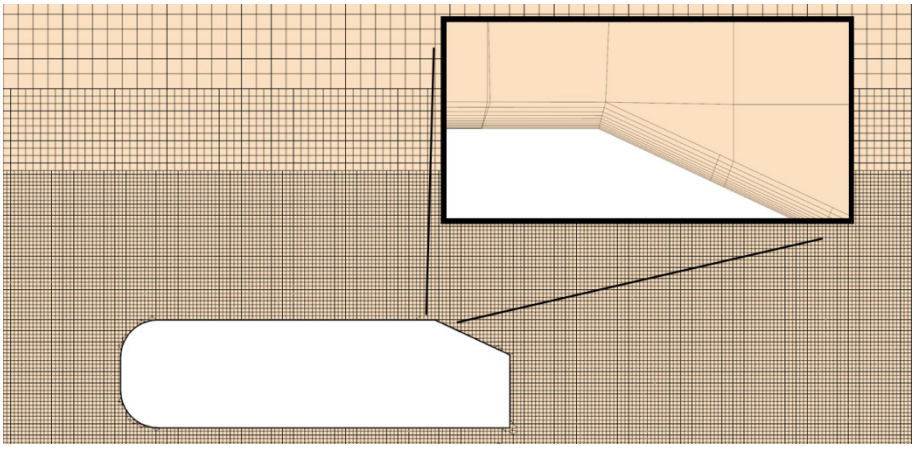

Fig. 3. Computational mesh.

After the mesh is drawn, the Y+ values at each point on the surface of the car body are shown in Fig. 4. The boundary layer setting of some parts of the model is reasonable. Most of the Y+ is less than 5, so the boundary layer setting is in line with the relevant calculation requirements.

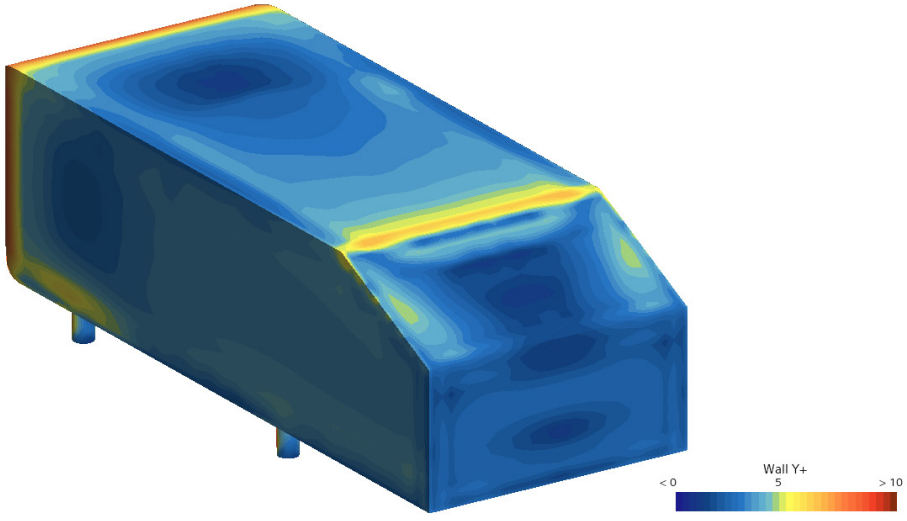

Fig. 4. Y+ on the vehicle surface.

2.4 Turbulence modelling

The fluid in the flow field is set as a constant-density airflow, and the inlet flow velocity is 40 m/s. Under this condition, the Reynolds number $Re=7.7\times10^5$ can be obtained by taking the length of the car body as the characteristic length. The turbulence model is the shear stress transport (SST) k-ω model. As a kind of widely-used turbulence model, the use of the k-ω model in the vicinity of the boundary layer can satisfy the relevant solution accuracy required by the present study, and the model evolved into the k-ε model in a position farther away from the boundary layer is also effective in avoiding the disadvantage of the k-ω model. It can meet the relevant solution accuracy required in this study by using the k-ω model near the boundary layer, while the k-ω model evolved to be the k-ε model at a more distant location from the boundary layer, which in turn effectively avoids the disadvantage of the k-ω model.

Fig. 5 shows its computational convergence curve in the absence of a jet in the above setup. The overall fluctuation of its various values after 2,600 steps is not significant, so in this paper , we will use the calculated average of 3,000

to 4,000 steps as the simulation results.

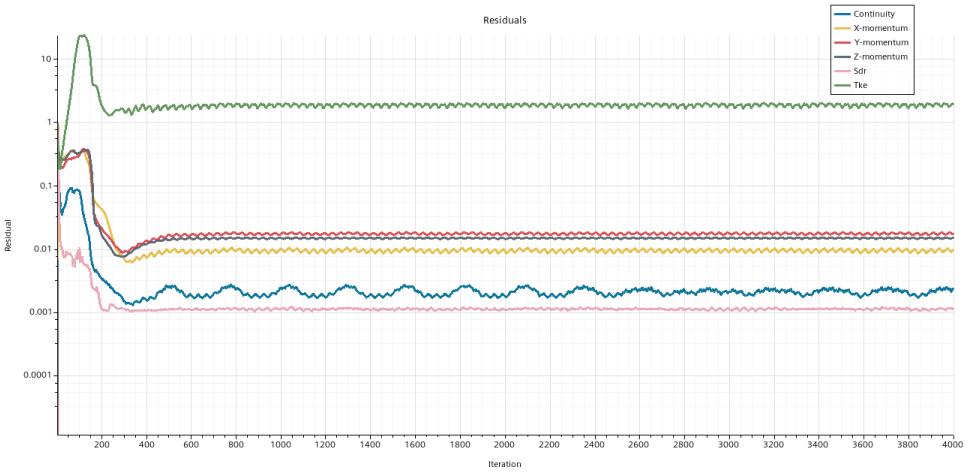

Fig. 5. Computational convergence curves without jet flow.

3. Results and discussion

3.1 On verification

For the working condition without blowing, two sets of grids with base meshes of 1,127,608 and 5,926,316 are plotted for calculations respectively. The forces in the x and z direction of the Ahmed body (drag and lift) in the calculation results are compared. Fig. 6 represents the calculation results of the three meshes. The aerodynamic fluctuations in the case of different grids are not more than 3.2% of the original grid, so it can be assumed in this case that the mesh plotting of the present subject will not have a significant impact on the specific experiments.

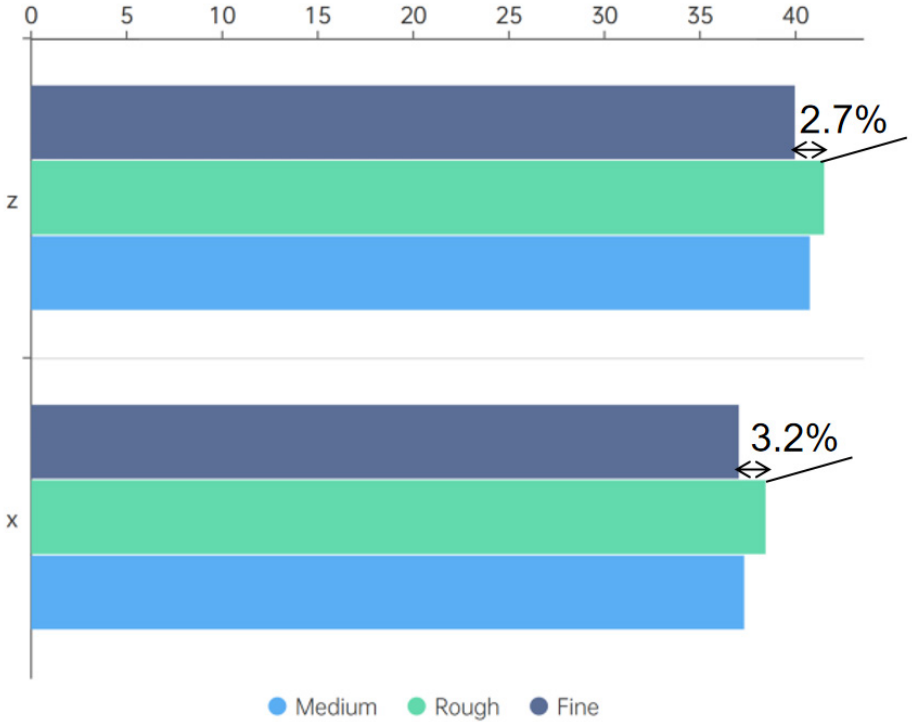

Fig. 6. Aerodynamic forces in x- and z-direction (drag and lift) on the Ahmed body at different mesh resolutions.

The drag coefficient of the Ahmed body obtained in this paper without blowing is 0.343, and the drag coefficient obtained by Rossitto et al. [10] through a wind tunnel test is 0.356 (Reynolds number of 7.17×10^5, which is close

to this paper). The difference between the two is 3.7%, indicating that the numerical method used in this paper is reliable.

3.2 Flow field without jet flow

We start with the flow field analysis of the model in the no-jet case, and Fig. 7 shows the velocity downstream of the Ahmed body in this case. The part of the model that contributes to the drag is concentrated in the tail of the model. The drag on the head is not analyzed because it is not within the scope of this study. Focusing on the tail part of the model, it can be seen that the airflow separates from the boundary layer on the slope of the back of the model, and the separation point is located at the corner of the back of the model. It can be verified from the pressures at various points on the upper surface of the model that the pressure of the airflow at the back decreases drastically after the boundary layer separation at the folding corner; the low-pressure region at the tail produces a relatively large drag force on the model.

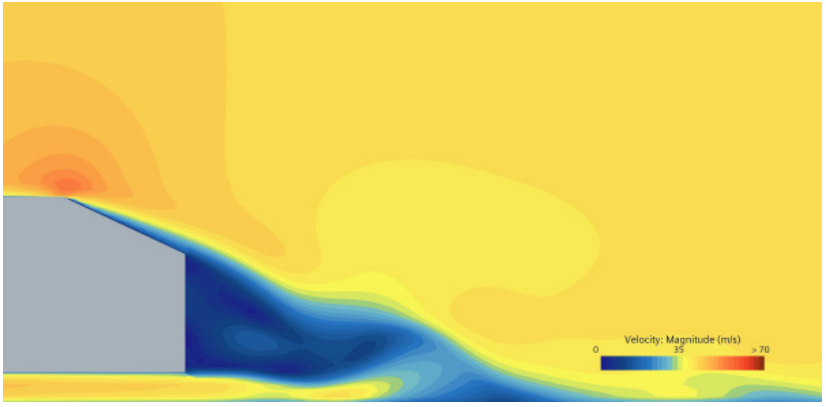

Fig. 7. Velocity downstream of the Ahmed body without the jet flow.

Fig. 8 shows the airflow streamlines at the rear of the vehicle without the jet flow, with the streamlines coloured according to velocity. The back of the model perpendicular to the x-axis produces a pair of counter-rotating vortices, and the vortex V0 as shown in the figure obviously occupies a dominant part compared to the lower part, and similar conclusions have been obtained by Xue et al. [7]. Therefore, injecting airflow into the low-pressure region downstream of the vehicle to reduce the low pressure at the back and directing the airflow to make the vortex V0 away from the back of the model can effectively reduce the vehicle drag.

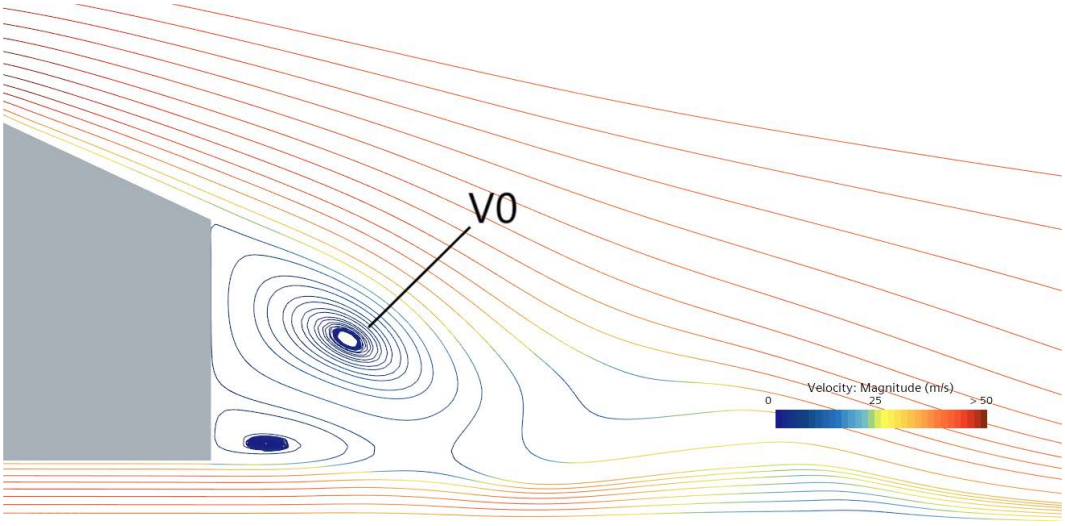

Fig. 8. Streamlines downstream of the Ahmed body without the jet flow.

3.3 Drag reduction effect by jet flow

3.3.1 Drag reduction effect at different jet velocities

Fig. 9 illustrates the aerodynamic drag of the vehicle for different jet velocities. The aerodynamic drag increases with the increase in jet velocity. When the jet velocity is 10 m/s, the aerodynamic drag decreases by 13.1% compared to the no-jet case.

When using the uppermost jet opening and jetting at velocities of 10 m/s, 20 m/s, and 30 m/s, respectively, normal to the jet plane, the simulation calculations yielded drag values of 32.4 N, 33.9 N, and 36.4 N in average, respectively (the drag of the vehicle without the jet flow is 37.3 N).

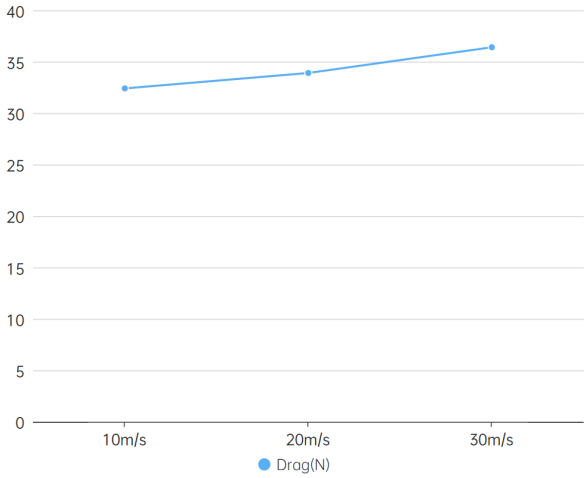

Fig. 9. Aerodynamic drag of vehicle at different jet velocities.

Fig. 10 shows the velocity downstream of the vehicle with a jet at different velocities. Compared with the condition without a jet, when the initial velocity of the jet opening is 10 m/s, the overall tail boundary layer separation point does not produce a very obvious change, but the overall trailing zone increases significantly and the velocity decreases. And when the jet velocity continues to increase. It can be clearly seen that the boundary layer separation point in the tail is advanced to before the dorsal slope. The earlier separation leads to more differential pressure resistance. Therefore, when the jet velocity increases significantly, the drag reduction effect is rather reduced.

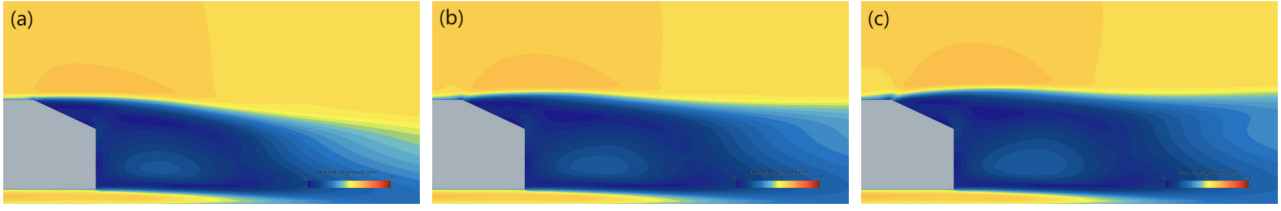

Fig. 10. Velocity of vehicle wake at different jet velocity: (a) jet velocity of 10 m/s, (b) jet velocity of 20 m/s, and (c) jet velocity of 30 m/s.

At the same time, in order to facilitate the analysis of the surface pressure of the Ahmed body, this paper selects the pressure at each point on the surface of the axial line in the model to be analyzed, and the location of the surface pressure on the body and the specific values of the pressure at each location are shown in Fig. 11 and Fig. 12.

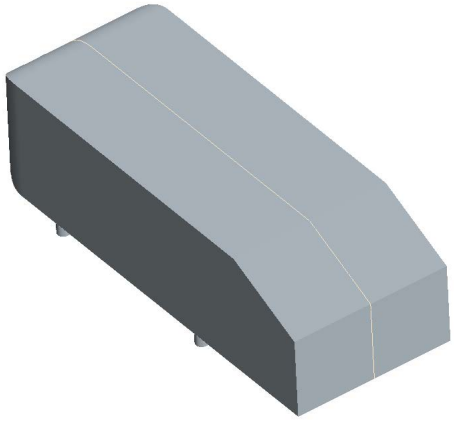

Fig. 11. Selection of the position of the pressure on the upper surface of the model.

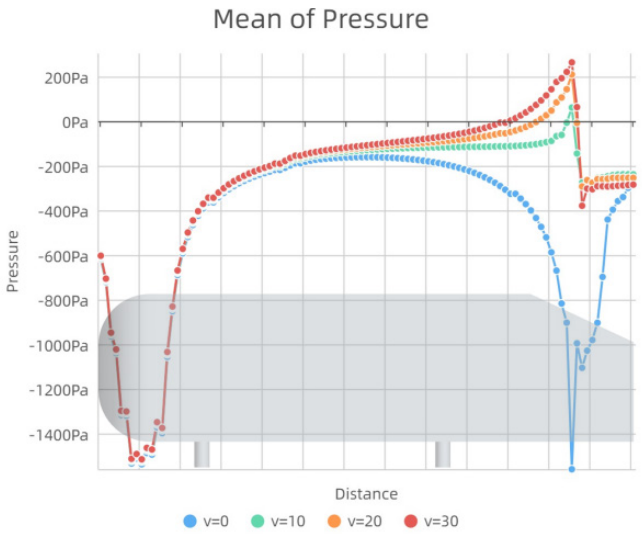

Fig. 12. Pressure values at points on the upper surface of the model.

This can be seen by the pressure conditions at various points on the body surface. In the absence of jet flow, a very obvious low-pressure area occurs at the dorsal fold corner. With the back velocity inlet jet, the low-pressure airflow generated by the boundary layer separation at the back is supplemented by the jet, so that the pressure reduction at the back corner is significantly reduced, and the position of the overall pressure drop is shifted back to the back slope. It can be seen that the back pressure reduction is the most obvious part of the jet drag reduction effect. With the increase of jet velocity, the back pressure will continue to increase, even in front of the folded corner to produce a certain high-pressure zone, but compared to the 10m/s jet compared to jet, the pressure increase is not very significant. At the same time, the above figure shows that the main location of the pressure increase compared to the 10m/s jet is more in front of the back slope, that is, the roof part of the car, and the pressure increase in this part of the airflow can not significantly affect the horizontal pressure difference resistance. This may be one of the reasons why the drag reduction effect does not continue to improve when the jet velocity continues to increase.

Fig. 13 shows the pressure values at various points on the surface of the rear slope of the Ahmed body in the no-jet case as well as in the case of jetting at different velocities. Compared to the case without the jet, the jet to the back can significantly enhance the low pressure generated at the back folds, thus achieving a more obvious drag reduction effect. When the jet speed is rising, its back pressure enhancement is not very obvious; this also confirms the conclusion that the drag reduction effect is not enhanced when the speed is rising.

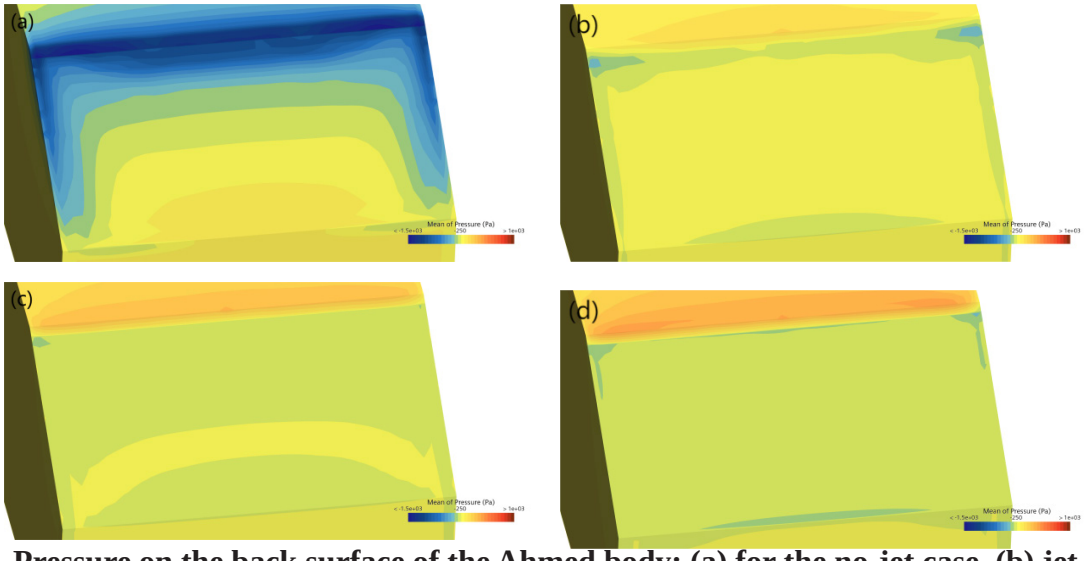

Fig. 13. Pressure on the back surface of the Ahmed body: (a) for the no-jet case, (b) jet velocity of 10 m/s, (c) jet velocity of 20 m/s, and (d) jet velocity of 30 m/s.

Fig. 14 represents the streamlines downstream of the vehicle. When the airflow is injected into the rear part of the vehicle by the injection port, the vortex V1 generated is obviously farther away from the rear part of the model compared with the vortex V0 in the no-jet state. This phenomenon can obviously improve the drag situation of the rear part of the vehicle. When the back jet velocity increases, the positions of the vortices V2 and V3 are not as V1 compared to V0 at a glance to produce a significant positional movement, it still stays in the back of the car space above. This phenomenon can also be interpreted in the jet velocity increases, the vehicle back resistance does not continue to reduce.

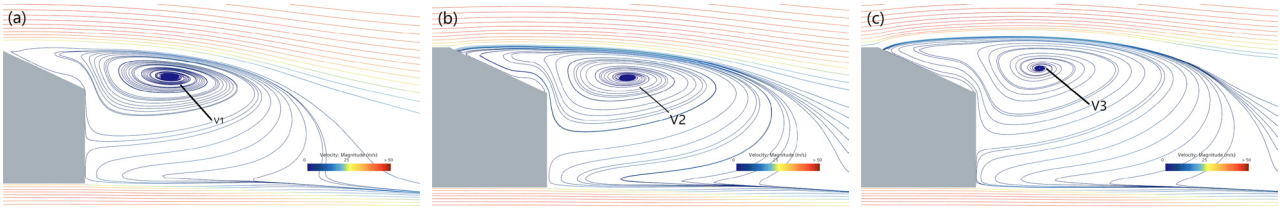

Fig. 14. Streamlines downstream of the Ahmed body at different jet velocities: (a) jet velocity of 10 m/s, (b) jet velocity of 20 m/s, and (c) jet velocity of 30 m/s.

3.3.2 Drag reduction at different jet positions

Fig. 15 illustrates the aerodynamic drag of the vehicle at different positions of the jet. The aerodynamic drag decreases as the jet position decreases. When the jet position is the lowest, the aerodynamic drag decreases by 16.4% compared to the no-jet case. At a fixed jet velocity of 20 m/s, the drag was calculated to be 33.9 N, 32.2 N, and 31.2 N by simulation when the top, middle, and bottom jet positions on the model were used for jetting, respectively.

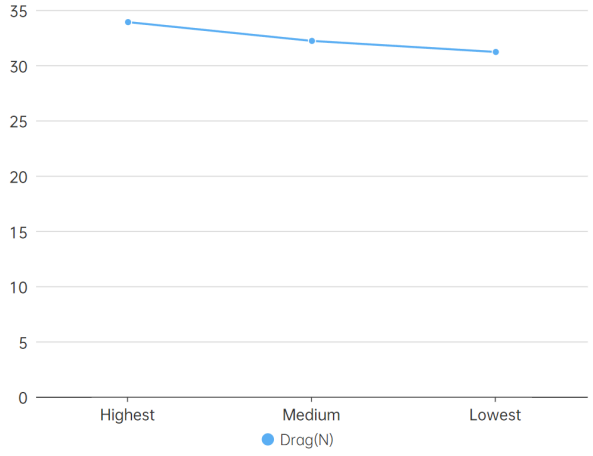

Fig. 15. Aerodynamic drag of vehicle at different jet positions.

Fig. 16 shows the flow velocity downstream of the Ahmed body when the jet velocity is fixed at 20 m/s for different locations of the jet at the rear of the model. When considering the case of different jets at different locations with the same velocity (20 m/s). Unlike the law that the low-velocity zone in the tail expands with increasing velocity, when the jet opening is away from the folding angle of the slope, the low-velocity flow in the tail will show a clear tendency to move towards the ground. At the same time , the separation point of the boundary layer will gradually move backward. It can be seen that when the jet opening is at position 1 or 2, the separation point of the boundary layer at the rear of the vehicle is kept in front of the folding angle; and when the position of the jet opening is moved to position 3, the separation point of the boundary layer at the rear of the vehicle coincides with that of the no-jet condition again, and the airflow separates in the position of the folding angle again.

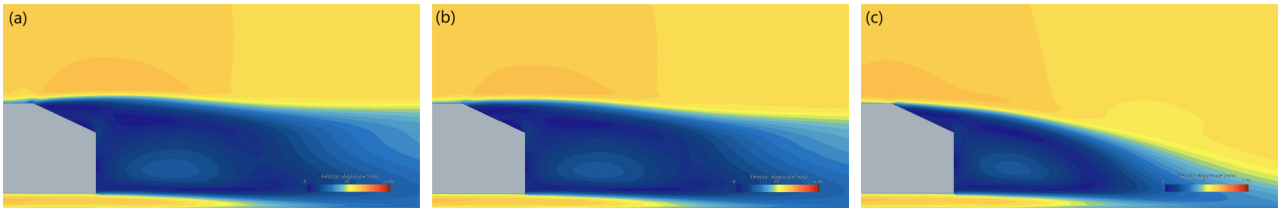

Fig. 16. Velocity downstream of the Ahmed body at different jet positions: (a) at P1, (b) at P2, and (c) at P3.

Fig. 17 presents the pressure at each point on the upper surface of the vehicle. As the jet position moves back, the peak pressure at the rear of the whole car also moves back. When the jet position is moved back to a certain degree, the pressure trend at the back of the car will change from the original increase before the folding corner to a rapid decrease before the folding corner and reach the lowest pressure at the folding corner, similar to the case without jet. However, the difference between this case (injection at position 3) and the no-injection case is that even though the pressure distribution trend is similar for the whole vehicle, in the injection case, the low pressure at the corner of the vehicle can still be reduced to a great extent: from the lowest pressure of less than -1400 Pa at the corner to about -600 Pa. So even though moving the injection point downwards brings the pressure trend behind the vehicle closer to the original pressure trend, there is still an excellent drag reduction effect.

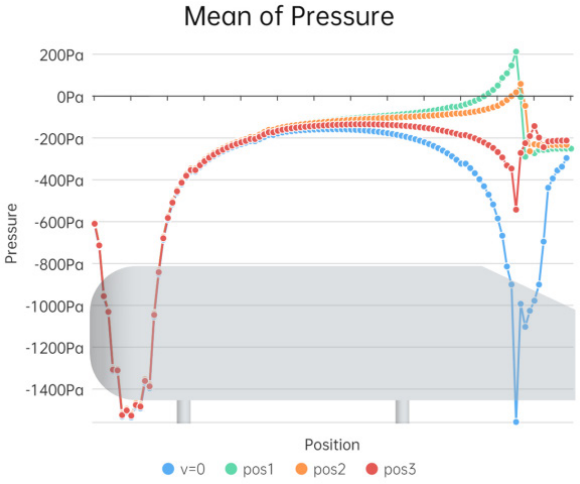

Fig. 17. Pressure on the upper surface of the model at different jet positions.

Fig. 18 represents the pressure on the back surface of the vehicle. The low-pressure zone at the back of the vehicle due to the boundary layer separation is greatly relieved in the case of the jets at positions 1 and 2, and a certain amount of high pressure is generated at the position in front of the folded corner, which is corroborated by the results of the pressure distribution maps at the points on the upper surface of the vehicle. When the injection port was moved to position 3, a low-pressure zone similar to that in the no-injection condition spreading from the middle corner to the sides was also seen at the folded corner. The pressure diagram at the slope position alone does not seem to explain why the jet at position 3 produces better drag reduction than the previous two.

Fig. 18. Surface pressures on the back of the model at different jet positions: (a) at P1, (b) at P2, and (c) at P3.

Considering that the differential pressure resistance at the back of the model does not only originate from the sloping surface at the back of the model, the plane perpendicular to the ground at its tail also still generates differential pressure resistance; therefore, Fig. 19 shows the surface pressure from the back of the Ahmed body for the relevant drag reduction analyses. However, from the rear view of the model, in addition to the low-pressure zone generated at the junction of the top surface of the model and the slope, a relatively small low-pressure zone is also generated at the slope and the backside of the vehicle body. From the rearview, generating jets at positions 1 and 2 can indeed provide better relief to the low-pressure zone at the top of the vehicle and the slope, but it cannot completely eliminate the low-pressure zone at the slope and the backside of the vehicle. The jet at position 3, on the other hand, can eliminate the low-pressure zone at the corner of the slope and the back of the slope better, although it does not increase the pressure of the low-pressure zone at the corner of the top and the slope as significantly as the former. At the same time, the pressure increase at the back of the vehicle is significantly better than in the two previous cases. Since the pressure generated by the backside pressure is in the same direction as the drag, boosting the pressure in this part of the vehicle can reduce the model drag very significantly.

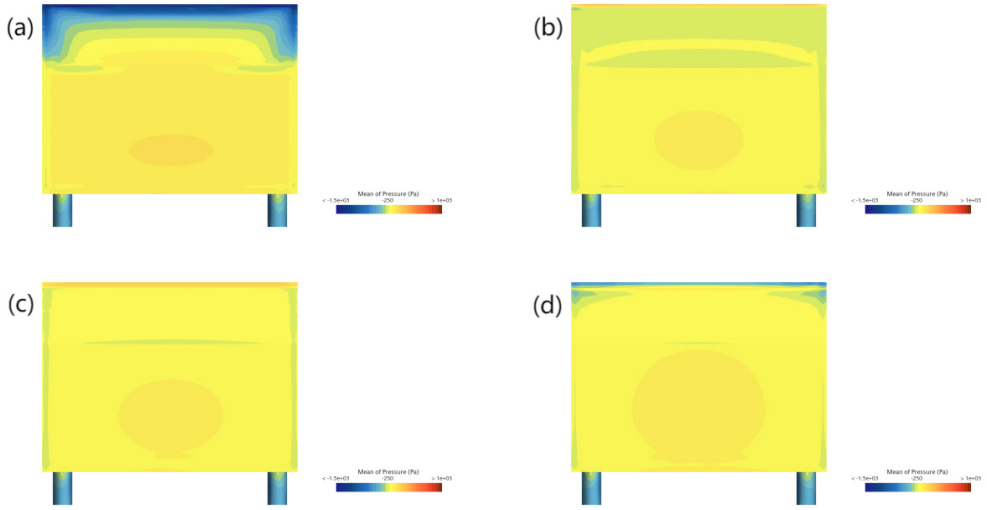

Fig. 19. Surface pressures directly behind the model at different jet positions: (a) in the case of no jet, (b) at P1, (c) at P2, and (d) at P3.

Fig. 20 shows the streamlines downstream of the vehicle model at different jet positions. The jet can dramatically change the position of the vortex at the rear of the model away from the body of the vehicle compared to the no-jet case. And when the jet exit is moved down, for vortices V5 and V6 in the figure, the position of the vortex does not change very much but moves slightly downward. Because under the jet condition, a large part of the kinetic energy of the vortices V5 and V6 are supplied by the jet outlet, so moving the jet outlet downward naturally results in the downward movement of the vortex. For the jet cases in Fig. 18(a) and (b), under the vortices V4 and V5, the back of the vehicle body will appear to a certain degree of low-pressure area, which can be seen in the back of the vehicle body flow line sparse, and when the vortex is moved down, due to the vortex is rotating clockwise, the vortex under the airflow can be just supplemented by the low-pressure airflow at the back of the vehicle, which will make it in the back of the overall pressure increase. This results page testifies to the results of the analysis of the pressure maps for the back of the vehicle.

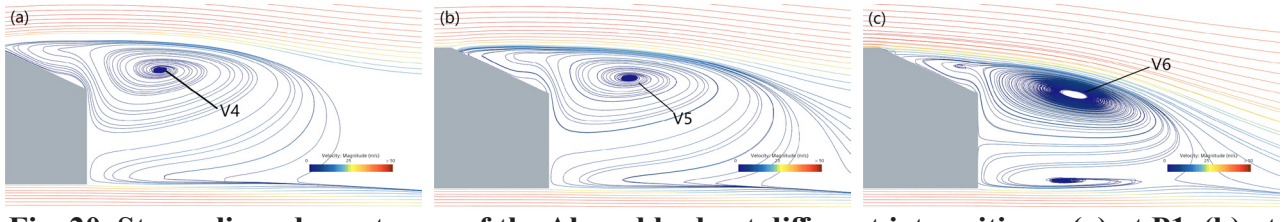

Fig. 20. Streamlines downstream of the Ahmed body at different jet positions: (a) at P1, (b) at P2, and (c) at P3.

4. Conclusions and outlooks

In this paper, for the aerodynamic characteristics of the 25° Ahmed body, different velocity jets are applied at different locations on its back slope to reduce its aerodynamic drag. Through simulation calculations, it can be seen that under normal conditions, the main resistance of the model comes from the differential pressure resistance at the back. The jet opening at the back airflow separation point can better relieve the differential pressure resistance, and when the airflow velocity is increasing, although theoretically there will be more mass of gas to supplement the low-pressure area at the back, it will also lead to the advancement of the position of the airflow separation point at the back of the model, and there is no significant increase in the pressure on the slope of the back of the model. At the same time, this paper also tries to move the position of the injection port downward from the corner of the slope of the model to compare and analyse the effect of injection at different positions; from the aerodynamic analysis of different injection ports, it can be seen that, although moving the injection port downward leads to the pressure at the separation point of the airflow is not as good as that of the injection at the separation point, the pressure at the front and back of the model is more obviously improved compared with that of injection at the upper edge of the slope. Therefore, the overall aerodynamic drag decreases with the downward movement of the jet opening. By comparing the two sets of experiments, it can be seen that the jetting scheme that takes into account the pressure on the front and back of the model as much as possible can achieve a better drag reduction effect in practical situations while ensuring that the separation point of the back boundary layer is not advanced.

From the simulation results, the downward movement of the jet opening, taking into account the pressure of the rear part of the Ahmed-type vehicle model perpendicular to the ground plane, also brings about a fairly objective drag reduction effect. In this paper, we do not continue to study the drag reduction effect of the model when the jet port is continuously moving downward, but for the consideration of the actual vehicle structure, the jet port is set up with the upper part of the model on the slanting back, which avoids the position of the rear windscreen of a normal vehicle. Therefore, the theoretical optimal location of the Ahmed model jet on the sloping back is still to be further investigated experimentally.

Due to the special characteristics of the jet system, there must be an air inlet to inhale an equal amount of airflow when jetting to the rear, and this paper does not make relevant assumptions and experimental verification of the influence of the air inlet on the drag reduction effect. Considering the arrangement of the air inlet in a suitable location, it may be able to achieve a better drag reduction effect. Meanwhile, the damping effect of this paper is mainly analysed in the steady state, but in reality, the Ahmed class vehicle model will have the situation of cyclic movement of the rear vortex under the steady incoming flow, and the jet damping method designed in this paper is not able to reduce the damping in this case, therefore, there is still room for further research in the future.

References

[1] Li Wenhuo. Study of Aerodynamic Drag Reduction Feature on Automobile with Non-smooth Groove Surface[D]. Zhejiang University,2014.

[2] HAECHEON C, JUNGIL L, HYUNGMIN P. Aerodynamics of heavy vehicles [J]. Annual Review of Fluid Mechanics, 2014, 46: 441. DOI: 10.1146/annurev-fluid-011212-140616.

[3] ZHANG Ya, WANG Hao, ZHANG Dan, et al. Study on drag reduction of automotive rearview mirror based on passive jet[J]. Journal of Jiangsu Institute of Technology,2022,28(04):66-74. DOI:10.19831/j.cnki.2095-7394.2022.04.006.

[4] YANG Zhigang, REN Jing, XIA Chao, et al. Active Drag Reduction of a SquareBack Ahmed Body with Wheels Based on Steady Blowing[J]. Journal of Tongji University (Natural Science Edition),2021,49(S1):39-47.

[5] AHMED S.R., RAMM G., FALTIN G. Some salient features of the time-averaged ground vehicle wake [J]. SAE Transactions, 1984, 93: 473-503. https://www.jstor.org/stable/44434262.

[6] Cui Liang. Study on aerodynamic resistance of Ahmed class vehicle body based on PERA SIM Fluid[J]. Industrial Technology Innovation,2023,10(06):19-27.DOI:10.14103/j.issn.2095-8412.2023.12.003.

[7] XUE Hongqiang, XU Bin, HUANG Diangui. Effect of flexible ribbon length on aerodynamic drag of Ahmed model [J]. Journal of Shanghai University of Technology,2024,46(01):52-59.DOI:10.13255/j.cnki.jusst.20221111002.

[8] ZHOU Haichao, CHEN Qingyun, LI Huiyun et al. Research on passive drag reduction method considering wake structure of an ahmed vehicle[J]. Journal of Chongqing University of Technology (Natural Science),2022,36(04):28-34.

[9] WANG Jingyu, GENG Yalin, HUIZHENG et al. Study on drag reduction of square-back vehicle model based on plasma flow control[J]. Automotive Engineering,2020,42(06):753-758+770.DOI:10.19562/j.chinasae.qcgc.2020.06.007.

[10] ROSSITTO Giacomo, SICOT Christophe, FERRAND Valérie et al. Influence of afterbody rounding on the pressure distribution over a fastback vehicle [J]. Experiments in Fluids, 2016, 57: 43. DOI: 10.1007/s00348-016-2120-1.